NIH Public Access
Author Manuscript
Cell Rep. Author manuscript; available in PMC 2013 April 03.

Published in final edited form as:
Cell Rep. 2013 March 28; 3(3): 831–843. doi:10.1016/j.celrep.2013.02.009.

Increased expression of enzymes of triglyceride synthesis is essential for the development of hepatic steatosis

Jingling Jin, **Polina Iakova**, **Meghan Breaux**, **Emily Sullivan**, **Nicole Jawanmardi**, **Dahu Chen**, **Yanjun Jiang**, **Estela M. Medrano**[1], and **Nikolai A. Timchenko**[1,*]

[1]Huffington Center on Aging and Departments of Pathology and Immunology and Molecular and Cellular Biology,Baylor College of Medicine, One Baylor Plaza, Houston, Texas 77030

Summary

Molecular mechanisms underpinning nonalcoholic fatty liver disease (NAFLD) are not well understood. The earliest step of NAFLD is hepatic steatosis, which is one of the main characteristics of aging liver. Here we present a molecular scenario of age-related liver steatosis. We show that C/EBPα-S193D knock-in mice have age-associated epigenetic changes and develop hepatic steatosis at 2 months of age. The underlying mechanism of the hepatic steatosis in old wild-type (WT) mice and in young S193D mice includes increased amounts of tripartite p300-C/EBPα/β complexes that activate promoters of five genes that drive triglyceride synthesis. Knock-down of p300 in old WT mice inhibits hepatic steatosis. Indeed, transgenic mice expressing dominant-negative p300 have fewer C/EBPα/β-p300 complexes and do not develop age-dependent hepatic steatosis. Notably, p300-C/EBPα/β pathway is activated in livers of patients with NAFLD. Thus, our results show that p300 and C/EBP proteins are essential participants in hepatic steatosis.

Keywords

Epigenetic; liver; steatosis; p300; C/EBP proteins

Introduction

Hepatic steatosis is the first step in the development of non-alcoholic fatty liver disease (NAFLD) and is characterized by accumulation of triglycerides (TGs) in the cytoplasm of hepatocytes. Hepatic steatosis can progress to non-alcoholic steatohepatitis (NASH), which is characterized by more severe liver damage. NASH, in turn, progresses to cirrhosis and, finally, to hepatocellular carcinoma (Cohen et al., 2011; Floreani, 2007; Hebbard and George, 2011; Schmucker, 2005). Indeed, elderly patients who develop hepatic steatosis are at high risk for developing liver cancer (Floreani, 2007; Schmucker, 2005; Timchenko, 2009). Therefore, the development of approaches to prevent or correct hepatic steatosis is important for improved health and extended lifespan in the elderly. The development of such approaches requires elucidation of the mechanisms that underlie hepatic steatosis. Diet-based animal models of NAFLD provide significant information regarding liver damage and

© 2013 Elsevier Inc. All rights reserved.

*Corresponding author: Nikolai A. Timchenko, Department of Pathology & Immunology and Huffington Center on Aging, Baylor College of Medicine, One Baylor Plaza, Houston, TX 77030, Tel: 713-798-1567, Fax: 713-798-4161, nikolait@bcm.tmc.edu.

Publisher's Disclaimer: This is a PDF file of an unedited manuscript that has been accepted for publication. As a service to our customers we are providing this early version of the manuscript. The manuscript will undergo copyediting, typesetting, and review of the resulting proof before it is published in its final citable form. Please note that during the production process errors may be discovered which could affect the content, and all legal disclaimers that apply to the journal pertain.

NIH-PA Author Manuscript
NIH-PA Author Manuscript
NIH-PA Author Manuscript

NIH-PA Author Manuscript

NIH-PA Author Manuscript

NIH-PA Author Manuscript

metabolic pathways of hepatic steatosis (Hebbard and George, 2011). Unfortunately, despite numerous studies of hepatic steatosis in these animal models of NAFLD, the mechanisms underlying hepatic steatosis remain unclear.

Transcription factor C/EBPα belongs to the C/EBP family of proteins, which are bZIP proteins containing a basic region and a leucine-zipper region (Johnson, 2005). bZIP proteins are transcription factors that dimerize with each other and control multiple functions in different tissues. We and other groups showed that C/EBPα is a strong inhibitor of liver proliferation (Flodby et al., 1996; Soriano et al., 1998; Timchenko et al., 1997; Wang et al., 2002; Wang et al., 2001). The biological activities of C/EBPα are regulated by protein-protein interactions and by post-translational modifications. Ser193, a key amino acid of C/EBPα, regulates multiple functions of C/EBPα and liver biology (Timchenko, 2009; Wang et al., 2006; Wang and Timchenko, 2005). The main finding of our long-term studies is that liver proliferation requires dephosphorylation of C/EBPα at Ser193 by the phosphoinositide 3′-kinase-Akt–protein phosphatase 2A (PP2A) pathway, whereas phosphorylation of this residue (p-Ser193) by cyclin D3–cdk4 stimulates the growth-inhibitory activity of C/EBPα. The p-Ser193 isoform of C/EBPα is abundant in livers of old mice and causes a number of age-related liver dysfunctions of the liver (Jin et al., 2010; Wang et al., 2010).

Histone modification (i.e., methylation or acetylation) regulates gene transcription. The acetylation state of histones is controlled by two classes of enzymes: histone acetyltransferases (HATs) and histone deacetylases (HDACs) (Giles et al., 1998; Lindemann et al., 2004). Histone hypo-acetylation is involved in a number of malignancies (Halkidou et al., 2004; Zhang et al., 2005). For example, mutations within the gene coding for the HAT p300 and a loss of heterozygosity at the p300 gene locus are associated with mammary tumors and glioblastomas (Giles et al., 1998). HDAC1 expression is increased in livers of old mice, leading to the formation of HDAC1-C/EBPα complexes and complexes with another C/EBP family member, C/EBPβ (Wang et al., 2008a,b). Although the role of p300 in aging is not understood, several recent papers show that p300 is involved in the development of cellular senescence. Li et al. demonstrated that p300 binds to the $p16^{INK4a}$ promoter and increases transcription of $p16^{INK4a}$ during cellular senescence (Li et al., 2011). p300 also contributes to cellular senescence through p53-independent and $p16^{INK4a}$-independent mechanisms (Prieur et al., 2011). In addition to transcriptional mechanisms, p300 might participate in senescence by acetylating proteins that regulate longevity (Dansen et al., 2009). In this article, we present a molecular mechanism for the age-associated development of steatosis. We use three genetically modified mouse models to show that p300-dependent regulation of chromatin structure during aging causes the activation of enzymes that synthesize TGs, leading to hepatic steatosis.

Results

C/EBPα-S193D mice develop steatosis at 2 months of age

C/EBPα is hyperphosphorylated at Ser193 in livers of old mice (Wang et al., 2006). We have generated C/EBPα-S193D knock-in mice (further called S193D mice) that express an age-associated isoform of C/EBPα (Jin et al., 2010; Wang et al., 2010). Young S193D mice are characterized by dramatic alterations similar to those observed in old mice, including alteration of chromatin structure with abundant heterochromatin regions (Jin et al., 2010). A change in the chromatin structure of S193D mice is shown in Supplemental Figure S1. One of the consequences of this change is the accumulation of TGs in the blood (Jin et al., 2010). Therefore, we have begun studies of the mechanisms and biological consequences of the elevation of TGs in S193D mice and in WT old mice. We stained livers of 2-month-old WT and S193D mice with Oil Red O. The livers of 2-month-old S193D mice developed steatosis

NIH-PA Author Manuscript

NIH-PA Author Manuscript

NIH-PA Author Manuscript

and had increased numbers of fat droplets in cytoplasm of hepatocytes (Fig. 1A). A comparison of Oil Red O–staining of livers of young S193D mice and livers of 24-month-old WT mice revealed that accumulation of fat droplets in S193D livers is similar to that observed in livers of old mice. Because TGs are the main components of fat droplets in steatotic livers, we examined the amount of TGs in livers and in blood of young S193D and old WT mice. TGs were increased in livers and in blood of S193D mice identical to that observed in old WT mice (Fig. 1B). Thus, young S193D mice mimic old WT mice in the development of hepatic steatosis and TG accumulation.

Increased expression of enzymes involved in TG synthesis in livers of young S193D mice and in livers of old WT mice

Young S193D and old WT mice have altered chromatin structure with numerous foci-like structures containing the marker of heterochromatin, histone H3 trimethylated at Lys9 (Jin et al., 2010). Therefore, we hypothesized that the alterations of chromatin structure cause increased production of TGs through several pathways including: 1) activation of genes involved in the synthesis of fatty acids; 2) activation of enzymes of TG synthesis; and 3) inhibition of genes involved in the degradation of TG. There were no significant differences in the expression of the lipogenic pathway enzymes FAS, ACC, and SCD1 or of fatty-liver uptake enzyme CD36 in livers of S193D mice as compared with those of WT mice (Supplemental Figure S2A). Likewise, we did not observe differences in the expression of HSL and ATGL (key enzymes of TG degradation) (Supplemental Figure S2B). Hepatic lipid analyses revealed no differences in the amounts of diacylglycerol, cholesterol, or free fatty acids (Supplemental Figure S3); however, we found a dramatic difference in the levels of enzymes that synthesize TGs. TGs are the end-product of a multistep synthetic pathway (Chen and Farese, 2005; Kantartzis et al., 2009), the last step of which is catalyzed by the CoA:diacylglycerol acyltransferases DGAT1 and DGAT2. The enzymes operating upstream of DGAT in TG synthesis are glycerol-phosphate acyltransferase (GPAT), acylglycerol-phosphate acyltransferase (AGPAT), phosphatidic acid phosphohydrolase–1 (PPH-1), and acyl CoA:monoacylglycerol acyltransferase (MGAT). We examined the expression of genes coding for these enzymes in livers of young S193D mice and in livers of old WT mice. Quantitative reverse transcription-polymerase chain reaction (Q-RT-PCR) revealed that expression of GPAT, AGPAT1, DGAT1, and DGAT2 mRNAs is increased in livers of young S193D and in livers of old WT mice (Fig. 1C). In addition, MGAT2 mRNA was increased in livers of S193D mice. Western blotting (Fig. 1D) and immunostaining (Fig. 1E) confirmed that DGAT1 and DGAT2 are increased in livers of young S193D mice and in livers of old WT mice. These results show that the transcription and translation of five TG-synthetic enzymes are increased in livers of young S193D and old WT mice. TG synthesis enzymes are also increased in adipose tissues of S193D mice and old WT mice (data not shown and Fig. 3D).

Because NAFLD is characterized by insulin resistance, which enhances hepatic fat accumulation by increasing free fatty acid delivery, we performed an insulin-resistance test and examined expression of the key gluconeogenic enzymes phosphoenol pyruvate carboxykinase (PEPCK) and glucose-6-phosphatase (G6Pase). These studies showed no significant differences in the insulin resistance or in expression of PEPCK and G6Pase in S193D mice as compared to WT mice (Supplemental Figure S4). S193D mice exhibit an early step of fatty liver disease: the accumulation of fat droplets in cytoplasm; however, other metabolic alterations, such as insulin resistance, might develop as these mice age, but they are not detectable in young S193D mice.

NIH-PA Author Manuscript

NIH-PA Author Manuscript

NIH-PA Author Manuscript

p300-C/EBPα/β complexes activate promoters of TG-synthetic genes during development of hepatic steatosis

We next determined the mechanisms that activate enzymes of TG synthesis in livers of aged WT mice and in livers of young S193D mice. The analysis of GPAT, MGAT2, AGPAT1, DGAT1, and DGAT2 promoters revealed that each of these promoters contains one or two C/EBP consensus binding sequences (Fig. 2A). C/EBPα and C/EBPβ proteins activate genes through the recruitment of p300 to their promoters (Erickson et al., 2001; Gaub et al., 2011); therefore, we hypothesized that p300-C/EBPα/β complexes might be involved in the activation of promoters of TG-synthetic genes. To test this supposition, we examined the interactions of C/EBPα and C/EBPβ with consensus binding sites within the promoters of GPAT, DGAT1, and DGAT2. Electrophoretic mobility shift assays showed that purified C/EBPα and C/EBPβ interact with DNA probes covering the C/EBP binding sites (data not shown). We next examined whether C/EBP proteins in liver nuclear extracts from S193D mice interact with these promoters. Use of specific antibodies showed that C/EBPα and C/EBPβ bind to these promoters as heterodimers because antibodies to each individual protein supershifted or neutralized all specific bands almost completely (Fig. 2B for the DGAT2 promoter). Thus, C/EBPα and C/EBPβ might control the promoters of genes of TG synthesis as heterodimers. To test this hypothesis, we performed chromatin immunoprecipitation (ChIP) assays using chromatin solutions from young WT, young S193D, and old WT mice with primers covering the C/EBP site in the DGAT1 and DGAT2 promoters. In livers of young WT mice, C/EBPα and C/EBPβ are observed on the DGAT1 and DGAT2 promoters, whereas p300 signals are not detectable. In livers of old WT mice and of young S193D mice, however, C/EBPα, C/EBPβ, and p300 are abundant on the DGAT1 and DGAT2 promoters (Fig. 2C). This recruitment of p300 leads to the acetylation of H3 at Lys9, demonstrating that the DGAT1 and DGAT2 promoters are activated in livers of young S193D mice and of old WT mice. A similar result was obtained for the GPAT promoter (data not shown).

Based on data from ChIP assays, we hypothesized that the C/EBPα/β dimers form complexes with p300 and that these complexes activate the TG synthesis genes. Examination of p300 and C/EBPα/β complexes using high-performance liquid chromatography (HPLC)-based size-exclusion chromatography showed that young WT mice contain low-MW complexes of C/EBPα with p300 and C/EBPβ. In young S193D mice, however, high-MW C/EBPα complexes are observed, which contain both p300 and C/EBPβ (Fig. 2D). Because C/EBPα and C/EBPβ heterodimers (Johnson, 2005; Timchenko, 2009) and because C/EBPα and C/EBPβ interact with the same region of p300 (CH3 domain, (Erickson et al., 2001; Gaub et al., 2011)), these data show that the high-MW complexes are formed by C/EBPα/β heterodimers and p300. To test whether C/EBPα/β heterodimers activate the gene promoters of TG-synthetic enzymes to a greater degree than do individual C/EBP proteins, we cloned DGAT1 and DGAT2 promoters into a pG3-luc reporter and cotransfected the promoters with individual C/EBP proteins or with C/EBPα +C/EBPβ together. Before performing these experiments, we established conditions for the efficient inhibition of p300 by siRNA (Supplemental Figure S5) and for appropriate molar ratios of transfected C/EBP genes (Fig. 2E). Using these conditions, we found that each individual protein activates the DGAT1 and DGAT2 promoters; however, the simultaneous expression of equal amounts of C/EBPα and C/EBPβ activates these promoters to a greater higher degree (Fig. 2F). The inhibition of p300 significantly reduces the ability of C/EBPα/β heterodimers to activate the DGAT1 and DGAT2 promoters (Fig. 2F). Together with data from the ChIP assays, these results demonstrate that C/EBPα/β heterodimers cooperate with p300 in the activation of the DGAT1 and DGAT2 promoters.

NIH-PA Author Manuscript

NIH-PA Author Manuscript

NIH-PA Author Manuscript

Inhibition of p300 in livers of old WT mice and knock-down of DGAT1 and DGAT2 in livers of young S193D mice inhibit hepatic steatosis

To determine whether hepatic steatosis in old WT mice and in young S193D mice involves the p300-DGAT1/2 pathway, we first inhibited p300 expression in the liver of old WT mice by siRNA. We used the in vivo–jetPei method of siRNA delivery (Polyplus transfection), which targets the injected siRNAs mainly to the liver and lung. After 1 week, animals were sacrificed and our investigation revealed that p300 expression was dramatically inhibited by siRNA in the liver but not in adipose tissue (Fig. 3A). The inhibition of p300 significantly reduced hepatic steatosis (Fig. 3B) and reduced the amount of TGs in the liver (Fig. 3C). These results indicate that the development of hepatic steatosis in WT old mice involves p300.

We next determined whether p300-mediated activation of DGAT1 and DGAT2 plays a causal role in development of hepatic steatosis in young S193D mice. We knocked down DGAT1 and DGAT2 expression using the siRNA technique described above and investigated liver steatosis at 7 days post inhibition. Western blotting showed that the amounts of DGAT1 and DGAT2 proteins are significantly inhibited by siRNAs in the liver, whereas the expression of these proteins was not affected significantly by siRNAs in adipose tissue (Fig. 3D). Oil Red O staining showed that the inhibition of both DGAT1 and DGAT2 concomitantly reduced the amount and size of the fat droplets (Fig. 3E) and amount of TGs in livers of S193D mice (Fig. 3F). Thus, increased expression of TG-synthetic enzymes in the liver of S193D mice is a key event in the development of hepatic steatosis.

High-fat diet (HFD) causes hepatic steatosis much faster in S193D knock-in mice than in WT mice

Because S193D mice have increased amounts of C/EBPα/β-p300 complexes, we examined whether S193D mice are more sensitive to developing hepatic steatosis when fed HFD. For these studies, we used 1-month-old mice because, at this age, S193D mice exhibit minor steatosis (Fig. 4A). WT and S193D mice were fed HFD for 3 and 12 weeks, and the development of hepatic steatosis was examined by several approaches. Hematoxylin and eosin (H&E) staining showed S193D livers contain a much greater number of fat droplets than do WT livers at 3 and 12 weeks of HFD. The most dramatic difference was observed at 3 weeks (Fig. 4A, left). Oil Red O staining confirmed these data and revealed that amount of fat droplets was significantly greater in livers of S193D mice treated with HFD (Fig. 4A, right). HFD also caused the increase of TG in the serum and in the livers of both WT and S193D mice, but this increase was greater in S193D mice (Fig. 4B and C). Because the differences in TG are associated with higher levels of enzymes of TG synthesis in S193D mice, we have examined expression of DGAT1 and DGAT2 proteins. Figure 4D shows that HFD increases the levels of these enzymes significantly higher in S193D mice than in WT mice. To confirm these observations, we stained the livers with DGAT2-specific antibodies. HFD led to increased DGAT2 in livers of S193D mice to a greater amount than that observed in livers of WT mice (Fig. 4E). These observations are consistent with the hypothesis that large amounts of C/EBPα/β-p300 complexes more strongly activate DGAT1 and DGAT2 promoters in S193D mice treated with HFD. Thus, these studies demonstrated that S193D mice develop hepatic steatosis under HFD conditions much faster and to a greater degree than do WT mice.

Transgenic mice expressing dominant-negative p300 do not develop age-associated steatosis

The p300 molecule contains several critical domains including a histone acetyltransferase domain, transactivation domains, and protein interaction domains CH1, CH2, and CH3 (Fig. 5A). The CH3 domain interacts with many transcription factors, including C/EBPα and C/

NIH-PA Author Manuscript

NIH-PA Author Manuscript

NIH-PA Author Manuscript

EBPβ, but does not have acetyltransferase and activation domains. Therefore, given that p300 participates in the activation of TG-synthetic genes, we generated transgenic mice that express the only CH3 domain of p300 (dnp300). A typical picture of genotyping is shown (Fig. 5B). The dnp300 transgenic mice were born normal and did not have visual abnormalities. A whole-body scan, however, revealed that the 12-month-old dnp300 transgenic mice display significantly less body fat than do WT mice (Fig. 5C). These results suggest that endogenous p300 is involved in increased fat storage and that dnp300 reduces this activity. We next examined accumulation of fat droplets in 20-month-old dnp300 and in control WT mice of the same age and found that 80%–95% of hepatocytes in the livers of old WT mice have fat droplets in cytoplasm (Fig. 5D). Only 15%–20% of hepatocytes in livers of 20-month-old dnp300 mice have cytoplasmic fat droplets. Thus, the examination of dnp300 mice indicates that p300 is required for the development of age-associated hepatic steatosis.

Dominant-negative p300 (dnp300) reduces the amount of p300-C/EBPα/β complexes in the liver

p300-C/EBPα/β complexes are important for the development of hepatic steatosis in S193D mice; therefore, we evaluated the hypothesis that dnp300 reduces hepatic steatosis through disruption of these complexes. To examine p300 and C/EBP complexes in old WT and old dnp300 mice, nuclear extracts were separated by size-exclusion chromatography, and fractions were scrutinized, as described in Fig. 2D. p300 was detected in all chromatographic fractions; however, p300 was not detected in high-MW fractions containing the proteins from dnp300 mice (Fig. 5E). Because dnp300 interacts with many transcription factors, we suggest that dnp300 disrupts high-MW complexes of WT p300 and its interacting proteins. It is also possible that the remaining amounts of p300 complexes are below the sensitivity threshold of our assays. In livers of old mice, C/EBPα is hyperphosphorylated at Ser193 (Wang et al., 2006; Wang and Timchenko, 2005) and forms high-MW complexes with chromatin remodeling proteins (Wang et al., 2008a; Wang et al., 2006). In agreement with previous observations, we found that the major fraction of C/EBPα from old WT mice existed in fractions containing high-MW complexes and that a portion of C/EBPβ was also detected in fractions containing high-MW complexes. On the contrary, in the extracts from dnp300 livers, both C/EBP proteins are found in the fractions containing low-MW complexes. Immunoprecipitating C/EBPα from each fraction and Western blotting with p300-specific and C/EBPβ-specific antibodies has shown that WT old mice contain high-MW p300-C/EBPα/β complexes and that these complexes are not detectable in livers of dnp300 mice. Notably, a portion of C/EBPα from livers of dnp300 mice is still observed in high-MW complexes that do not contain p300. This portion perhaps represents previously characterized complexes of C/EBPα with HDAC1 and Brm (Wang et al., 2008b; Wang et al., 2006). Thus, these studies demonstrate that dnp300 disrupts complexes of endogenous WT p300 with C/EBPα/β. Consistent with the lack of p300-C/EBPα/β complexes, dnp300 mice are resistant to the development of hepatic steatosis under HFD (Fig. 5F).

Double S193D-dnp300 mice are resistant to developing HFD-mediated hepatic steatosis

To further examine the role of dnp300 in inhibition of steatosis, we crossed S193D and dnp300 mice, and the double hetero-S193D-dnp300 mice (further called S193D-dnp300) were used for the experiments on HFD-mediated steatosis. Figure 6A shows genotyping of S193D-dnp300 mice. We treated these mice and WT mice with HFD and examined development of hepatic steatosis at 3 and 12 weeks. Intriguingly, the S193D-dnp300 livers looked different from WT livers at 12 weeks after initiation of HFD, showing less white color (Fig. 6B). H&E and Oil Red O staining showed that livers of S193D-dnp300 mice are resistant to the development of steatosis within 12 weeks of HFD treatment (Fig. 6C).

NIH-PA Author Manuscript

NIH-PA Author Manuscript

NIH-PA Author Manuscript

Immunostaining of WT and S193D-dnp300 livers with DGAT1-specific and DGAT2-specific antibodies revealed that HFD significantly increased the expression of these enzymes in WT mice, but the elevation of DGAT1 and DGAT2 was lower in livers of S193D-dnp300 mice (Fig. 6D, DGAT1 results not shown). ChIP assays using the DGAT1 and DGAT2 promoters showed that HFD-treated WT mice exhibited recruitment of p300 to both promoters, followed by acetylation of histone H3 at Lys9. In S193D-dnp300 mice, however, HFD treatments did not lead to the recruitment of endogenous p300 to the promoters (Fig. 6E and F, upper images). ChIP assays using antibodies specific for a c-myc epitope, which is fused to dnp300 (Fig. 5), showed that c-myc–dnp300 occupied the DGAT1 and DGAT2 promoters in livers of S193D-dnp300 mice after HFD treatments. This occupation was associated with the inhibition of the promoters because histone H3 is trimethylated at Lys9 on the promoters (Fig. 6E and F, bottom images).

p300-C/EBPα-DGAT2 pathway is activated in patients with fatty liver disease

We next asked whether p300-C/EBPα/β pathway is utilized in human patients with fatty liver diseases. The key step in the development of hepatic steatosis in mice includes hyperphosphorylation of C/EBPα at S193 and subsequent formation of C/EBPα-p300 complexes. Therefore, we first examined whether phosphorylation of the human C/EBPα is increased in patients with fatty liver diseases. The human C/EBPα (serine is located in position 190) has significant differences in the amino-acid sequence flanking Ser190 (Fig. 7A), and antibodies to mouse p-Ser193 C/EBPα do not recognize human C/EBPα. Therefore, we generated antibodies that specifically interact with the human p-Ser190 isoform of C/EBPα. Western blotting showed that the p-Ser190 isoform of human C/EBPα is abundant in human fatty livers and that treatment of protein extracts with PP2A [which removes the phosphate from this serine (Wang et al., 2004)], eliminating the interaction of the antibody with C/EBPα protein (Fig. 7A). In tissue sections from six patients with fatty liver disease and tissue sections from four healthy livers of age-matched patients, we found the p-Ser190 isoform of human C/EBPα is detectable in a few hepatocytes of normal patients whereas up to 90% of hepatocytes from fatty livers contain the p-Ser190 isoform of C/EBPα (Fig. 7B and C). We next examined whether p-Ser190 C/EBPα colocalized with p300 in livers of patients with NAFLD and observed two major differences between normal and NAFLD livers: an increased number of hepatocytes with colocalized p300 and p-Ser190-C/EBPα in NAFLD and an increased number of hepatocytes with multiple sites of colocalizations of p-Ser190-C/EBPα and p300 (Fig. 7D and Supplemental Figure S6). The number of hepatocytes with p300-C/EBPα complexes increased approximately 45% in patients with NAFLD, whereas in normal livers, the increase was approximately 5%. The number of hepatocytes with multiple colocalizations of C/EBPα and p300 increased in patients with NAFLD and represents approximately 25% of hepatocytes. We tested the amount of DGAT2 (the downstream target of the C/EBPα-p300 complexes) present and found it increased in p300-C/EBPα–positive hepatocytes from NAFLD livers (Fig. 7E). Thus, these results reveal that the p300-C/EBPα-DGAT2 pathway is activated in patients with fatty liver disease.

Discussion

The molecular mechanisms that underpin age-associated development of steatosis are not well understood. Several recent publications revealed that alterations of the chromatin structure occur in livers of old mice (Jin et al., 2010; Kreiling et al., 2011; Wang et al., 2010), suggesting that this change might be involved in hepatic steatosis. In this paper, we examined this hypothesis using several genetically modified animal models and WT young and old mice. Because C/EBPα is hyperphosphorylated at Ser193 in livers of old mice, we generated C/EBPα-S193D mice, which mimics age-like isoform of C/EBPα, and showed

NIH-PA Author Manuscript

NIH-PA Author Manuscript

NIH-PA Author Manuscript

that this age-like mutation causes several changes in liver physiology similar to those observed in old mice (Jin et al., 2010). Comparison of the TG amounts in livers of young S193D mice and in old WT mice revealed that the increase in S193D mice was similar to those observed in livers of old mice and that young S193D mice develop steatosis in a similar manner to that in old WT mice. Thus, these observations suggested that molecular mechanisms of the steatosis in young S193D mice might be similar to those in age-associated hepatic steatosis in WT mice. Further examination of this hypothesis showed that these mechanisms are identical and include the activation of the gene promoters of TG-synthetic enzymes by p300-C/EBPα/β complexes. The critical role of p300 in the development of hepatic steatosis is shown by experiments with siRNA to p300 (Fig. 3) and by examination of three genetically modified animal models: S193D mice, dnp300 mice, and double S193D-dnp300 mice. Our hypothesis for the mechanisms underlying age-associated hepatic steatosis (Fig. 7) is supported by previous studies demonstrating that expression C/EBPα and C/EBPβ is altered in livers of old mice (Timchenko et al., 2006; Wang et al., 2006). Further support is provided by our findings that the amounts of p300-C/EBPα/β are increased in livers of young S193D mice and in livers of old WT mice. Examination of the gene promoters of the key TG synthesis enzymes GPAT, DGAT1, and DGAT2 showed that p300-C/EBPα/β activates these promoters during the development of hepatic steatosis in several animal models. The disruption of the p300-C/EBPα/β complexes by dnp300 blocks the activation of the DGAT1 and DGAT2 promoters and correlates with the inhibition of the age-associated steatosis and with inhibition of steatosis initiated by HFD.

Several high-affinity C/EBP consensus binding sites exist in the gene promoters of five TG-synthetic enzymes. Although both DGAT1 and DGAT2 are important modulators of energy metabolism (Yen et al., 2008), DGAT2 appears to be the dominant DGAT enzyme controlling TG homeostasis in vivo (Stone et al., 2004). DGAT2-deficient (*Dgat2*$^{-/-}$) mice survive for only a few hours after birth. In contrast, *Dgat1*$^{-/-}$ mice are viable and have an approximately 50% reduction in adiposity (Smith et al., 2000; Tsai et al., 2007), maintain a lean phenotype even on HFD, and are resistant to diet-induced obesity (Smith et al., 2000). Studies in transgenic mice confirmed that overexpression of either DGAT enzyme can cause TG accumulation of cytosolic lipid droplets in the liver (Monetti et al., 2007). The reduction of DGAT2 by antisense oligonucleotide improves hepatic steatosis and hyperlipidemia in obese mice (Yu et al., 2005). Consistent with literature data showing the critical roles of DGAT1 and DGAT2, our studies with knocking down the expression of these enzymes revealed that the increase in DGAT1 and DGAT2 is the main pathway of the steatosis development in S193D mice. The mechanistic studies in this paper were focused on the liver; however, we also showed that expression of enzymes of TG synthesis is increased in adipose tissues (Fig. 3). We suggest that alterations of adipose tissues also contribute to development of steatosis. However, because inhibition of DGAT1 and DGAT2 in the liver was sufficient to block steatosis in S193D mice, we think that elevation of enzymes of TG synthesis in the liver is critical for hepatic steatosis. Importantly, we observed that the C/EBPα-p300-DGAT2 pathway is activated in patients with NAFLD. These findings suggest that the inhibition of C/EBPα-p300 pathways might be considered a therapeutic approach to prevent the development of hepatic steatosis.

Experimental Procedures

Animal Experiments

Experiments with animals were approved by the Institutional Animal Care and Use Committee at Baylor College of Medicine (protocol AN-1439). We have used WT young (2–4 months), WT old (22–24 months), young C/EBPα-S193D and S193D-dnp300 mice. Generation and characterization of C/EBPα-S193D mice were described in previous papers

NIH-PA Author Manuscript

NIH-PA Author Manuscript

NIH-PA Author Manuscript

(Jin et al., 2010; Wang et al., 2010). Livers were harvested and kept at −80°C. Mice were fed either a standard laboratory chow diet or HFD (D12331, Research Diets, New Brunswick, NJ) for 3 or 12 weeks. Data in the manuscript are obtained with 3–5 mice per experiment with three to four independent repeats.

Generation of transgenic mice expressing dominant-negative CH3-p300 (dnp300) and double knock-in transgenic S193D-dnp300 mice

To generate transgenic mice that express the CH3 domain of p300, we used the chicken β-actin promoter plus the CMV-IE enhancer to clone a 993-bp cDNA from the mouse p300 gene. To examine the dnp300 molecule in further experiments, the CH3 domain was fused to a c-myc epitope tag (Fig. 5A). Genotyping analysis was performed using primers: Forward: 5′-AGC ACC ACG TGG AGA CAC GC-3′; Reverse: 5′-GGC AGG GAG CAG TTG GCG TT-3′. To obtain S193D-dnp300 mice, we crossed homozygous S193D mice and dnp300 mice. We used heterozygous S193D-dnp300 mice because further crossing of these heterozygous mice with homozygous S193D mice reduced the amount of dnp300 expressed.

Human samples from patients with fatty liver disease

We used six tissues sections from patients with fatty liver disease obtained from OriGene Technologies. Four tissue sections from normal patients were used as the controls.

Liver histology and immunohistochemistry

The livers were fixed overnight in buffered 10% formaldehyde, embedded in paraffin, and sectioned at a thickness of 4 μm. The sections were stained with H&E using a standard protocol or with different antibodies against DGAT1 (ab54037, Abcam) or DGAT2 (ab96094, Abcam). For Oil Red O staining, the 7-μm liver cryosections were stained with commercially available kits (IW-3008, IHC World).

Biochemical assays

Serum TGs were measured in facilities at Baylor College of Medicine. Liver TGs were quantified by commercially available kits (ab65336, Abcam)

Antibodies and Reagents

Antibodies used were specific for C/EBPβ (C-19), C/EBPα (14AA), DGAT1 (H-255), DGAT2 (H-70), ATGL (H-144), HSL (H-300), P300 (N-15 or C-20) (Santa Cruz Biotechnology), for AGPAT (4613) (Prosci, Inc., for DGAT1 (ab54037) and DGAT2 (ab96094) (Abcam), and for acetyl-histone H3 (9649s) and histone H3 trimethyl Lys9 (9754s) (Cell Signaling). Monoclonal anti-β-actin antibody was from Sigma. P300 small interfering RNA (siRNA, sc-29431) and control siRNA-A were from Santa Cruz Biotechnology.

Cotransfection studies

Hep3B2 cells were transfected using the Fugene 6 transfection reagent (Roche Molecular Biochemicals) according to the manufacturer's protocol. Forty-eight hours after transfection, a luciferase assay was performed using the Dual-Luciferase Reporter Assay System (Promega). Luciferase activity was normalized by the Renilla internal control.

Protein isolation and Western blotting

Protein extracts were isolated from livers of young and old mice as described previously (Jin et al., 2009; Wang et al., 2004). Inhibitors of phosphatases were included in all buffers used for the isolation of proteins or protein-protein complexes. Proteins (50–100 μg) were loaded

NIH-PA Author Manuscript

NIH-PA Author Manuscript

NIH-PA Author Manuscript

on gradient (4%–20% Bio-Rad) polyacrylamide gels, transferred onto membranes, and probed with antibodies against proteins of interest. To verify protein loading, each filter was re-probed with β-actin–specific antibody.

Chromatin immunoprecipitation assay

ChIP assays were performed using the ChIP It kit as described previously (Jin et al., 2009; Wang et al., 2008b; Wang et al., 2007). Briefly, chromatin solutions were prepared from livers of young, old, and HFD mice. C/EBPα, C/EBPβ, p300, acetyl-histone H3 (Lys9), and trimethyl-histone H3 (Lys9) were immunoprecipitated from the solutions. The sequences of primers used in the ChIP assay are shown in Supplemental Materials.

Examination of p300-C/EBPα/β complexes by size-exclusion chromatography

P300-C/EBPα/β complexes were isolated by HPLC-based chromatography of nuclear extracts on SEC400 column (BioRad) as described previously (Wang et al., 2006). Briefly, 1.5–2 mg of nuclear extracts was loaded on the SEC400 column. Fractions were collected and analyzed by Western blotting with antibodies to C/EBPα, C/EBPβ, and p300. C/EBPα was immunoprecipitated from each fraction, and C/EBPβ and p300 were examined in these IPs.

Real-time quantitative reverse transcription-polymerase chain reaction

Total RNA was isolated from mouse livers using RNeasy Plus mini kit (QIAGEN) according to the manufacturer's instructions. cDNA was synthesized using an oligo(dT) primer and Superscript III reverse transcriptase (Invitrogen). The real-time PCR mixtures contained 1× Brilliant II SYBR green QPCR master mix (Stratagene), 200 nM of each primer, 1× ROX dye (Invitrogen), and the synthesized cDNA. PCR amplification was performed in triplicate in a 96-well plate for each sample on an ABI PRISM 7000 sequence detection system (Applied Biosystems). The relative expressions were normalized to β-actin. The sequences of PCR primers are shown in Supplemental Materials.

Supplementary Material

Refer to Web version on PubMed Central for supplementary material.

Acknowledgments

This work was supported by NIH grants GM551888, CA100070, AG039885, AG032135, AG028865, and CA159942 (NAT). We thank Adam Antebi for discussion of the results and Sharra Hammond for help with genotyping of dnp300 mice.

References

Chen HC, Farese RV Jr. Inhibition of triglyceride synthesis as a treatment strategy for obesity: lessons from DGAT1-deficient mice. Arterioscler Thromb Vasc Biol. 2005; 25:482–486. [PubMed: 15569818]

Cohen JC, Horton JD, Hobbs HH. Human fatty liver disease: old questions and new insights. Science. 2011; 332:1519–1523. [PubMed: 21700865]

Dansen TB, Smits LM, van Triest MH, de Keizer PL, van Leenen D, Koerkamp MG, Szypowska A, Meppelink A, Brenkman AB, Yodoi J, et al. Redox-sensitive cysteines bridge p300/CBP-mediated acetylation and FoxO4 activity. Nat Chem Biol. 2009; 5:664–672. [PubMed: 19648934]

Erickson RL, Hemati N, Ross SE, MacDougald OA. p300 coactivates the adipogenic transcription factor CCAAT/enhancer-binding protein alpha. J Biol Chem. 2001; 276:16348–16355. [PubMed: 11340085]

NIH-PA Author Manuscript

NIH-PA Author Manuscript

NIH-PA Author Manuscript

Flodby P, Barlow C, Kylefjord H, Ahrlund-Richter L, Xanthopoulos KG. Increased hepatic cell proliferation and lung abnormalities in mice deficient in CCAAT/enhancer binding protein alpha. J Biol Chem. 1996; 271:24753–24760. [PubMed: 8798745]

Floreani A. Liver diseases in the elderly: an update. Dig Dis. 2007; 25:138–143. [PubMed: 17468549]

Gaub P, Joshi Y, Wuttke A, Naumann U, Schnichels S, Heiduschka P, Di Giovanni S. The histone acetyltransferase p300 promotes intrinsic axonal regeneration. Brain. 2011; 134:2134–2148. [PubMed: 21705428]

Giles RH, Peters DJ, Breuning MH. Conjunction dysfunction: CBP/p300 in human disease. Trends Genet. 1998; 14:178–183. [PubMed: 9613201]

Halkidou K, Gaughan L, Cook S, Leung HY, Neal DE, Robson CN. Upregulation and nuclear recruitment of HDAC1 in hormone refractory prostate cancer. Prostate. 2004; 59:177–189. [PubMed: 15042618]

Hebbard L, George J. Animal models of nonalcoholic fatty liver disease. Nat Rev Gastroenterol Hepatol. 2011; 8:35–44. [PubMed: 21119613]

Jin J, Wang GL, Iakova P, Shi X, Haefliger S, Finegold M, Timchenko NA. Epigenetic changes play critical role in age-associated dysfunctions of the liver. Aging Cell. 2010; 9:895–910. [PubMed: 20698834]

Jin J, Wang GL, Shi X, Darlington GJ, Timchenko NA. The age-associated decline of glycogen synthase kinase 3beta plays a critical role in the inhibition of liver regeneration. Mol Cell Biol. 2009; 29:3867–3880. [PubMed: 19398579]

Johnson PF. Molecular stop signs: regulation of cell-cycle arrest by C/EBP transcription factors. J Cell Sci. 2005; 118:2545–2555. [PubMed: 15944395]

Kantartzis K, Machicao F, Machann J, Schick F, Fritsche A, Haring HU, Stefan N. The DGAT2 gene is a candidate for the dissociation between fatty liver and insulin resistance in humans. Clin Sci (Lond). 2009; 116:531–537. [PubMed: 18980578]

Kreiling JA, Tamamori-Adachi M, Sexton AN, Jeyapalan JC, Munoz-Najar U, Peterson AL, Manivannan J, Rogers ES, Pchelintsev NA, Adams PD, et al. Age-associated increase in heterochromatic marks in murine and primate tissues. Aging Cell. 2011; 10:292–304. [PubMed: 21176091]

Li N, Li Q, Cao X, Zhao G, Xue L, Tong T. The tumor suppressor p33ING1b upregulates p16INK4a expression and induces cellular senescence. FEBS Lett. 2011; 585:3106–3112. [PubMed: 21896275]

Lindemann RK, Gabrielli B, Johnstone RW. Histone-deacetylase inhibitors for the treatment of cancer. Cell Cycle. 2004; 3:779–788. [PubMed: 15153801]

Monetti M, Levin MC, Watt MJ, Sajan MP, Marmor S, Hubbard BK, Stevens RD, Bain JR, Newgard CB, Farese RV Sr, et al. Dissociation of hepatic steatosis and insulin resistance in mice overexpressing DGAT in the liver. Cell Metab. 2007; 6:69–78. [PubMed: 17618857]

Prieur A, Besnard E, Babled A, Lemaitre JM. p53 and p16(INK4A) independent induction of senescence by chromatin-dependent alteration of S-phase progression. Nat Commun. 2011; 2:473. [PubMed: 21915115]

Schmucker DL. Age-related changes in liver structure and function: Implications for disease ? Exp Gerontol. 2005; 40:650–659. [PubMed: 16102930]

Smith SJ, Cases S, Jensen DR, Chen HC, Sande E, Tow B, Sanan DA, Raber J, Eckel RH, Farese RV Jr. Obesity resistance and multiple mechanisms of triglyceride synthesis in mice lacking Dgat. Nat Genet. 2000; 25:87–90. [PubMed: 10802663]

Soriano HE, Kang DC, Finegold MJ, Hicks MJ, Wang ND, Harrison W, Darlington GJ. Lack of C/EBP alpha gene expression results in increased DNA synthesis and an increased frequency of immortalization of freshly isolated mice [correction of rat] hepatocytes. Hepatology. 1998; 27:392–401. [PubMed: 9462636]

Stone SJ, Myers HM, Watkins SM, Brown BE, Feingold KR, Elias PM, Farese RV Jr. Lipopenia and skin barrier abnormalities in DGAT2-deficient mice. J Biol Chem. 2004; 279:11767–11776. [PubMed: 14668353]

NIH-PA Author Manuscript

NIH-PA Author Manuscript

NIH-PA Author Manuscript

Timchenko LT, Salisbury E, Wang GL, Nguyen H, Albrecht JH, Hershey JW, Timchenko NA. Age-specific CUGBP1-eIF2 complex increases translation of CCAAT/enhancer-binding protein beta in old liver. J Biol Chem. 2006; 281:32806–32819. [PubMed: 16931514]

Timchenko NA. Aging and liver regeneration. Trends Endocrinol Metab. 2009; 20:171–176. [PubMed: 19359195]

Timchenko NA, Harris TE, Wilde M, Bilyeu TA, Burgess-Beusse BL, Finegold MJ, Darlington GJ. CCAAT/enhancer binding protein alpha regulates p21 protein and hepatocyte proliferation in newborn mice. Mol Cell Biol. 1997; 17:7353–7361. [PubMed: 9372966]

Tsai J, Qiu W, Kohen-Avramoglu R, Adeli K. MEK-ERK inhibition corrects the defect in VLDL assembly in HepG2 cells: potential role of ERK in VLDL-ApoB100 particle assembly. Arterioscler Thromb Vasc Biol. 2007; 27:211–218. [PubMed: 17038630]

Wang GL, Iakova P, Wilde M, Awad S, Timchenko NA. Liver tumors escape negative control of proliferation via PI3K/Akt-mediated block of C/EBP alpha growth inhibitory activity. Genes Dev. 2004; 18:912–925. [PubMed: 15107404]

Wang GL, Salisbury E, Shi X, Timchenko L, Medrano EE, Timchenko NA. HDAC1 cooperates with C/EBPalpha in the inhibition of liver proliferation in old mice. J Biol Chem. 2008a; 283:26169–26178. [PubMed: 18622015]

Wang GL, Salisbury E, Shi X, Timchenko L, Medrano EE, Timchenko NA. HDAC1 promotes liver proliferation in young mice via interactions with C/EBPbeta. J Biol Chem. 2008b; 283:26179–26187. [PubMed: 18622014]

Wang GL, Shi X, Haefliger S, Jin J, Major A, Iakova P, Finegold M, Timchenko NA. Elimination of C/EBPalpha through the ubiquitin-proteasome system promotes the development of liver cancer in mice. J Clin Invest. 2010; 120:2549–2562. [PubMed: 20516642]

Wang GL, Shi X, Salisbury E, Sun Y, Albrecht JH, Smith RG, Timchenko NA. Cyclin D3 maintains growth-inhibitory activity of C/EBPalpha by stabilizing C/EBPalpha-cdk2 and C/EBPalpha-Brm complexes. Mol Cell Biol. 2006; 26:2570–2582. [PubMed: 16537903]

Wang GL, Shi X, Salisbury E, Sun Y, Albrecht JH, Smith RG, Timchenko NA. Growth hormone corrects proliferation and transcription of phosphoenolpyruvate carboxykinase in livers of old mice via elimination of CCAAT/enhancer-binding protein alpha-Brm complex. J Biol Chem. 2007; 282:1468–1478. [PubMed: 17107955]

Wang GL, Timchenko NA. Dephosphorylated C/EBPalpha accelerates cell proliferation through sequestering retinoblastoma protein. Mol Cell Biol. 2005; 25:1325–1338. [PubMed: 15684384]

Wang H, Goode T, Iakova P, Albrecht JH, Timchenko NA. C/EBPalpha triggers proteasome-dependent degradation of cdk4 during growth arrest. EMBO J. 2002; 21:930–941. [PubMed: 11867521]

Wang H, Iakova P, Wilde M, Welm A, Goode T, Roesler WJ, Timchenko NA. C/EBPalpha arrests cell proliferation through direct inhibition of Cdk2 and Cdk4. Mol Cell. 2001; 8:817–828. [PubMed: 11684017]

Yen CL, Stone SJ, Koliwad S, Harris C, Farese RV Jr. Thematic review series: glycerolipids. DGAT enzymes and triacylglycerol biosynthesis. J Lipid Res. 2008; 49:2283–2301. [PubMed: 18757836]

Yu XX, Murray SF, Pandey SK, Booten SL, Bao D, Song XZ, Kelly S, Chen S, McKay R, Monia BP, et al. Antisense oligonucleotide reduction of DGAT2 expression improves hepatic steatosis and hyperlipidemia in obese mice. Hepatology. 2005; 42:362–371. [PubMed: 16001399]

Zhang Z, Yamashita H, Toyama T, Sugiura H, Ando Y, Mita K, Hamaguchi M, Hara Y, Kobayashi S, Iwase H. Quantitation of HDAC1 mRNA expression in invasive carcinoma of the breast*. Breast Cancer Res Treat. 2005; 94:11–16. [PubMed: 16172792]

NIH-PA Author Manuscript

NIH-PA Author Manuscript

NIH-PA Author Manuscript

Highlights

- Epigenetic alterations correlate with hepatic steatosis in old mice
- Increase of enzymes of TG synthesis is involved in age-related steatosis
- p300-C/EBPα/β complexes cause activation of enzymes of TG synthesis
- p300-C/EBP pathway is activated in patients with NAFLD

NIH-PA Author Manuscript
NIH-PA Author Manuscript
NIH-PA Author Manuscript

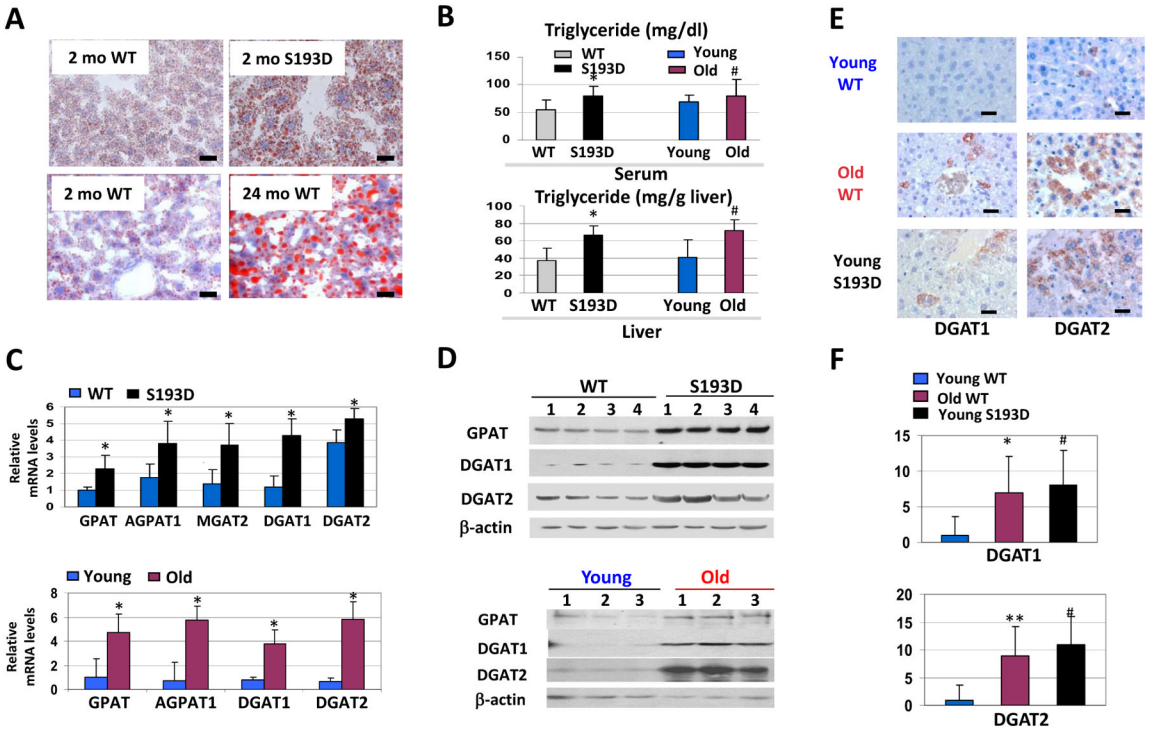

Figure 1.

Young S193D mice develop hepatic steatosis at the age of 2 months. **A.** Livers of 2-month-old (young) S193D mice and livers of 24-month-old WT mice were stained with Oil Red O. Scale bars: 10 μm. **B.** Amounts of TG in serum (upper) and liver (bottom) of young S193D and old WT mice are increased. Bar graphs show results of the analyses with eight mice of each genotype and each age group. * $p<0.05$, S193D versus WT, # $p<0.05$ old versus young. **C.** mRNA levels of enzymes of TG synthesis are increased in livers of S193D mice and in livers of old WT mice. Q-RT-PCR was performed with RNA isolated from livers of young WT and S193D mice (upper image) and from livers of WT old mice (bottom image). **D.** Protein levels of GPAT, DGAT1, and DGAT2 are increased in livers of S193D mice. Western blotting was performed with protein extracts isolated from the livers of young WT and S193D mice (upper) and old WT mice (bottom). Each membrane was re-probed with antibodies to β-actin. **E.** Immunostaining of livers of young WT, young S193D and old WT mice with antibodies to DGAT1 and to DGAT2. Note that livers of old WT mice and young S193D mice have enlarged hepatocytes (Jin et al., 2010). Scale bar: 10 μm. **F.** The number of DGAT1- and DGAT2-positive hepatocytes in livers of young WT, young S193D, and old WT mice. Bar graphs show the results of analyses of three animals of each group. * $p<0.05$, ** $p<0.01$, old WT versus young WT, # $p<0.05$ young S193D versus young WT.

NIH-PA Author Manuscript

NIH-PA Author Manuscript

NIH-PA Author Manuscript

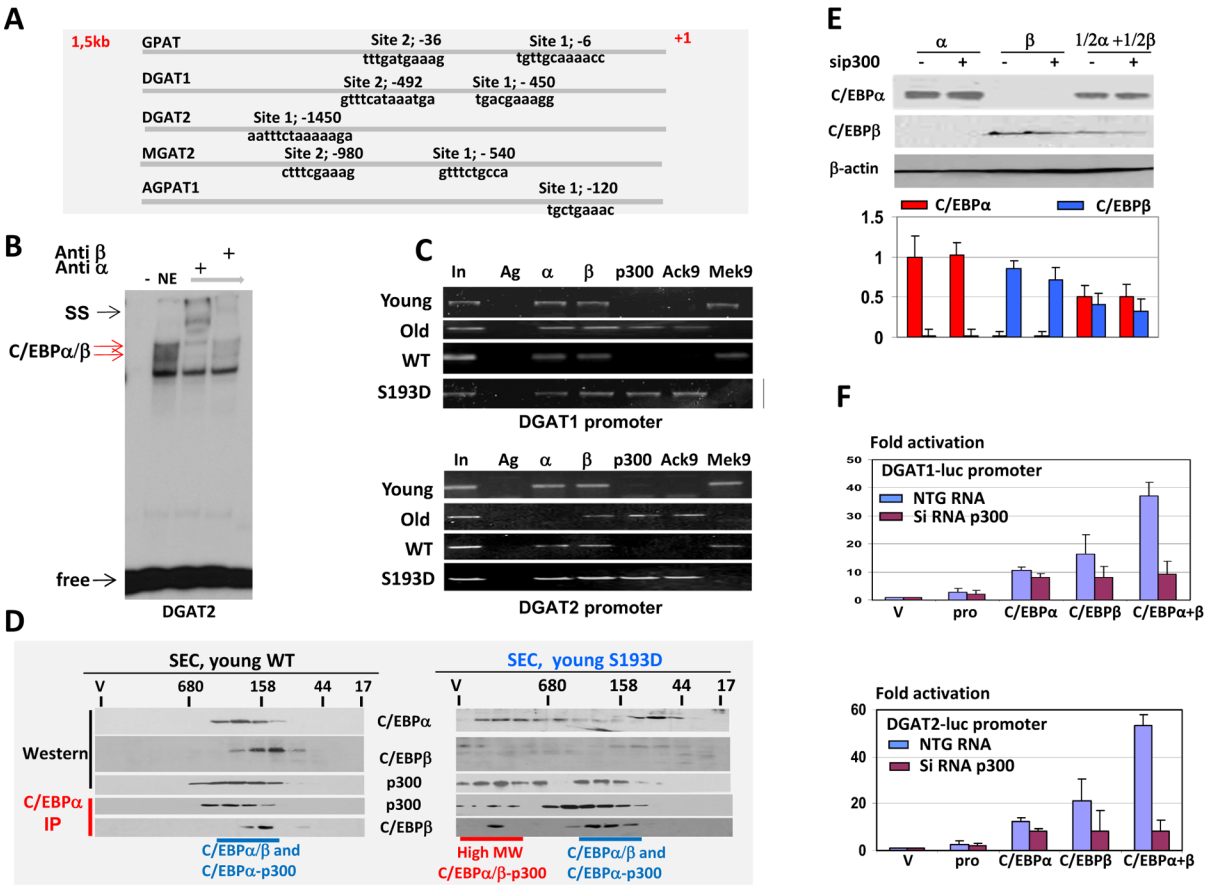

Figure 2.

p300-C/EBPα/β complexes occupy and activate the gene promoters driving TG-synthetic enzyme expression in livers of S193D mice. **A.** Promoters of GPAT, DGAT1, DGAT2, MGAT2, and AGPAT1 contain C/EBP sites. Locations and sequences of C/EBP having sites are shown. **B.** Electrophoretic mobility shift assay performed with the DGAT2 probe and nuclear extracts from S193D mouse livers. Antibodies to C/EBPαμ and C/EBPβ were included in the binding reactions. Positions of C/EBPα/β complexes and supershift (SS) are shown. **C**. C/EBP proteins recruit p300 to DGAT1 and DGAT2 promoters in livers of S193D mice and in livers of old WT mice. C/EBPα, C/EBPβ, p300, histone H3 acetylated at Lys9, or trimethylated on Lys9 were immunoprecipitated from chromatin solutions and examined in PCR reactions with primers amplifying C/EBP sites on the DGAT1 and DGAT2 promoters. In; 1/100 input. **D**. High-MW p300-C/EBPα/β complexes are abundant in livers of young S193D mice. Nuclear extracts from WT and S193D livers were separated by size-exclusion chromatography. The position of size-exclusion markers is shown at the top. Location of the p300 and C/EBP proteins in the fractions was determined by Western blotting with specific antibodies. C/EBPα-IP; C/EBPα was immunoprecipitated from each fraction and p300 and C/EBPβ were detected in these IPs. **E.** Amounts of C/EBPα and C/EBPβ proteins in cells transfected with individual DNAs coding for α, β, or both. In the case where both α and β were transfected, one-half the amount used in the single (α or β) transfections was used so that the total transfected equaled the amount used singly in α or β. Total lysates were isolated and examined by Western blotting with antibodies to C/EBPα and C/EBPβ. Bar graphs: Levels of C/EBP proteins were calculated as ratios to β-actin. **F.** p300-C/EBPα/β heterodimers activate the DGAT1 (upper) and DGAT2 (bottom) promoters more strongly than do individual C/EBPα and C/EBPβ proteins. DGAT1-luc and DGAT2-

luc reporter constructs were cotransfected with constructs expressing C/EBPα, C/EBPβ, or both proteins. A similar experiment was performed in cells with inhibited p300. Data in Fig. 2E and F represent summary of 3–4 independent experiments.

NIH-PA Author Manuscript
NIH-PA Author Manuscript
NIH-PA Author Manuscript

NIH-PA Author Manuscript

NIH-PA Author Manuscript

NIH-PA Author Manuscript

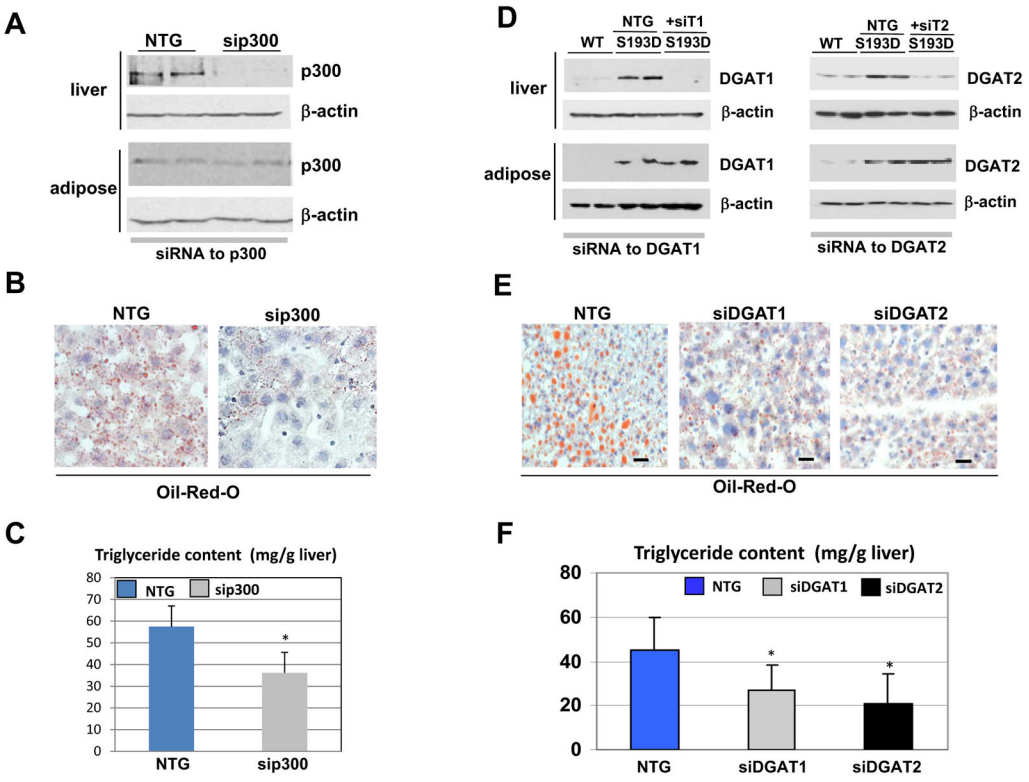

Figure 3.

p300 and p300-mediated elevation of DGAT1 and DGAT2 are responsible for the development of hepatic steatosis in old WT mice and in young S193D mice. **A.** Inhibition of p300 by siRNA in livers of old WT mice. Western blotting shows p300 in liver and in adipose tissues of mice treated with p300-specific siRNA and with control non-targeting RNA (NTG). β-actin is a control for protein loading. **B.** Oil Red O staining of livers of old WT mice treated with NTG and with siRNA to p300. **C.** Amounts of TG in livers of old WT mice treated with siRNA to p300. Bar graph is an average of 3 independent experiments. **D.** Knock-down of DGAT1 and DGAT2 inhibits hepatic steatosis in S193D mice. Western blotting was performed using antibodies to DGAT1 and DGAT2 with protein extracts isolated from liver and adipose tissues. β-Actin shows protein loading. NTG, treatments of S193D mice with control non-targeting RNA. **E.** A typical picture of Oil Red O staining of livers at 7 days after delivery of DGAT1 and DGAT2 siRNAs. NTG; treatments of WT and S193D mice treated with non-specific RNA. **F.** Bar graphs show amounts of TG in the livers of mice treated with DGAT1 and DGAT2 siRNAs as an average of three independent experiments.

NIH-PA Author Manuscript

NIH-PA Author Manuscript

NIH-PA Author Manuscript

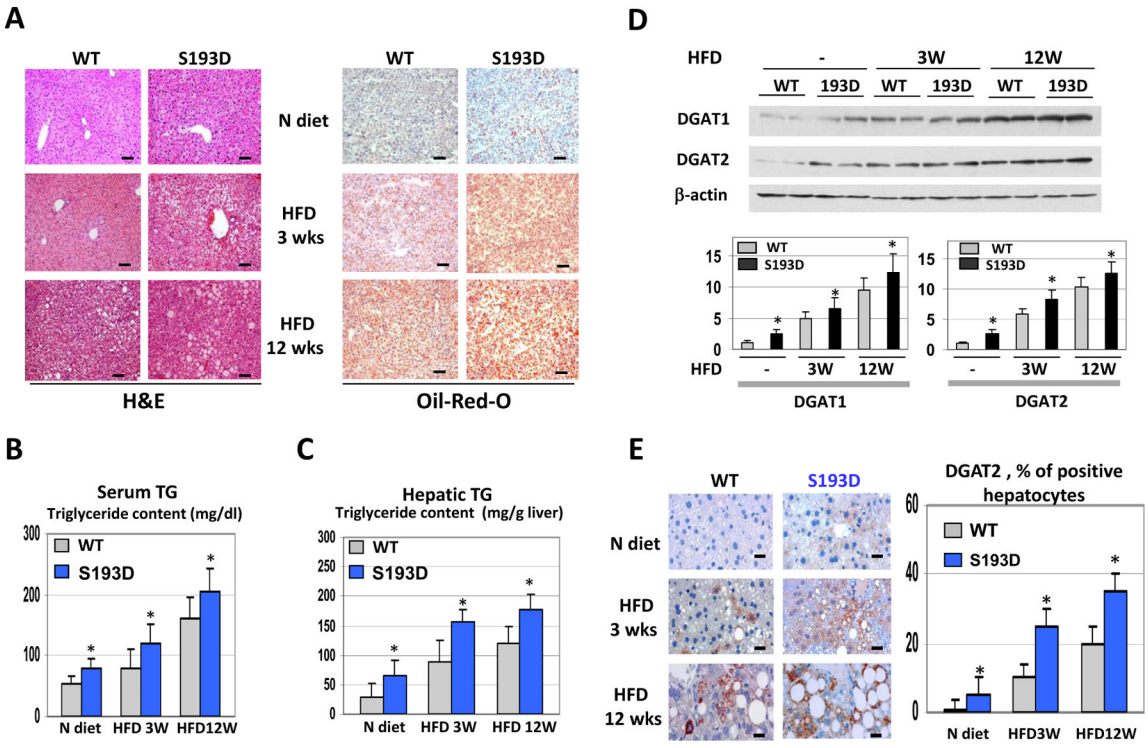

Figure 4.

Development of hepatic steatosis by HFD is accelerated in S193D mice. **A.** A typical picture of H&E (left) and Oil Red O (right) staining of WT and S193D livers under HFD conditions. Upper image shows staining of the livers under normal diet (N diet). Scale bar: 40 μm. **B and C.** Amounts of TGs in serum and in livers of WT and S193D mice at different time points of HFD. Data from three animals of each genotype are presented as bar graphs. **D.** Amounts of DGAT1 and DGAT2 in livers after HFD. Western blotting was performed with protein extracts isolated at 3 and 12 weeks after initiation of HFD. Bar graphs show ratios of DGAT1 and DGAT2 to β-actin. **E.** Examination of DGAT2 expression in livers of WT and S193D mice by immunostaining. Bar graphs show the number of DGAT2-positive hepatocytes in livers of WT and S193D mice. Scale bar: 10 μm.

NIH-PA Author Manuscript

NIH-PA Author Manuscript

NIH-PA Author Manuscript

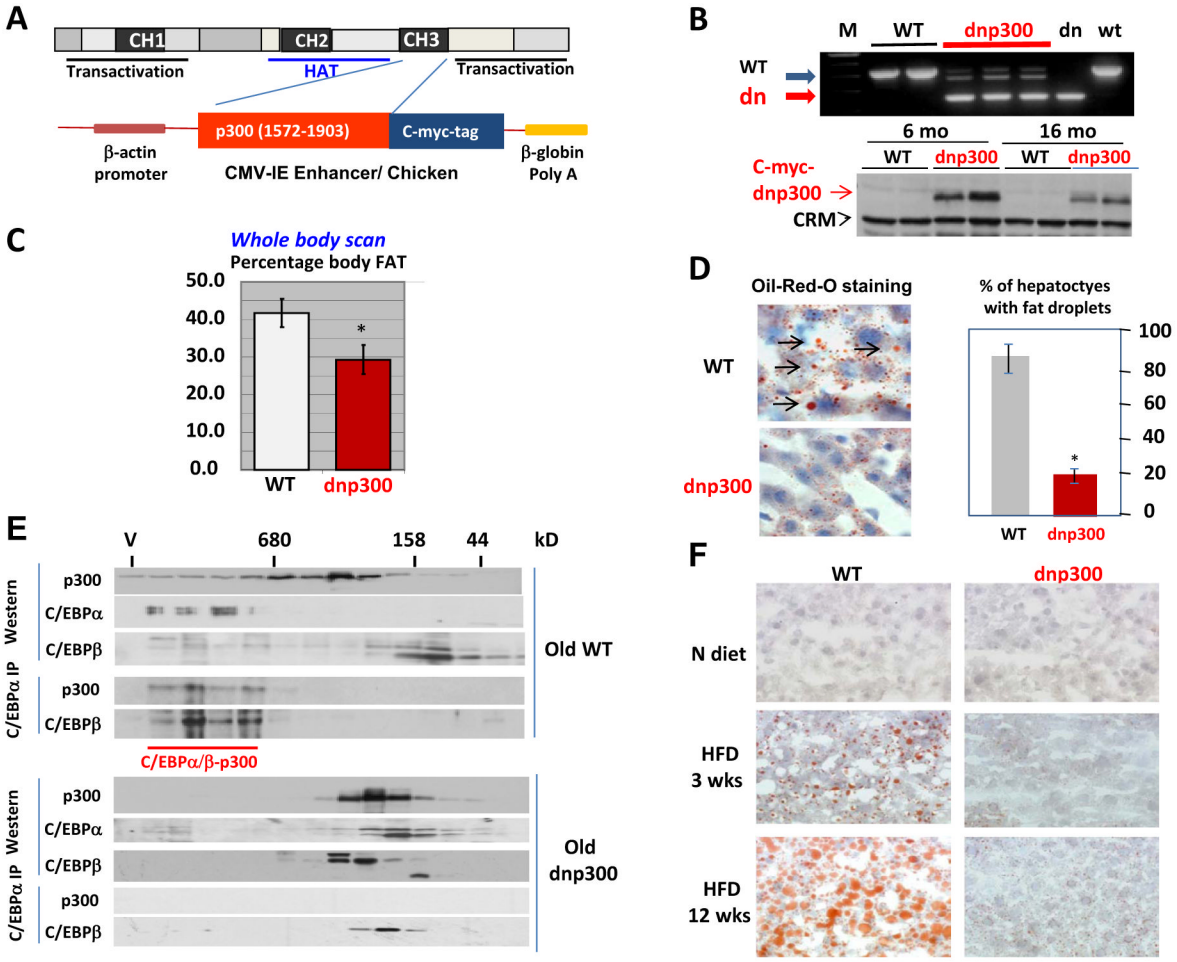

Figure 5.

Transgenic mice expressing dominant-negative p300 (dnp300) do not develop hepatic steatosis with age and under HFD conditions. **A.** Generation of transgenic animals expressing dnp300. Scheme showing the localization of the CH3 domain used in the generation of the transgenic animals. **B.** PCR genotyping gel indicating three animals display genomic insertion of the transgene. Dn and wt; PCR from control plasmids containing dominant-negative and WT cDNAs. Western blotting (bottom image) shows expression of c-myc–dnp300 in livers of transgenic animals. CRM; cross reactive molecule. **C.** The total fat is reduced in transgenic mice. **A** whole-body scan was performed on WT and dnp300 mice. Bar graphs represent an average of 5 animals of each genotype. **D.** Numbers of fat droplets are reduced in livers from dnp300 mice (20 months of age) as compared with the numbers WT animals (20 months of age). Hepatocytes from WT or dnp300 mice were stained with Oil Red O. The number of hepatocytes with fat droplets was calculated in livers of WT and dnp300 mice. The bar graph picture shows a summary of three repeats with five animals of each genotype. **E.** dnp300 disrupts C/EBPα/β-p300 complexes in livers of old mice. Protein extracts from livers of 20-month-old WT and dnp300 mice were separated on the SEC400 column. Fractions were analyzed as described in the legend to Fig. 2D. **F.** dnp300 mice do not develop hepatic steatosis within 12 weeks of HFD protocol.

NIH-PA Author Manuscript

NIH-PA Author Manuscript

NIH-PA Author Manuscript

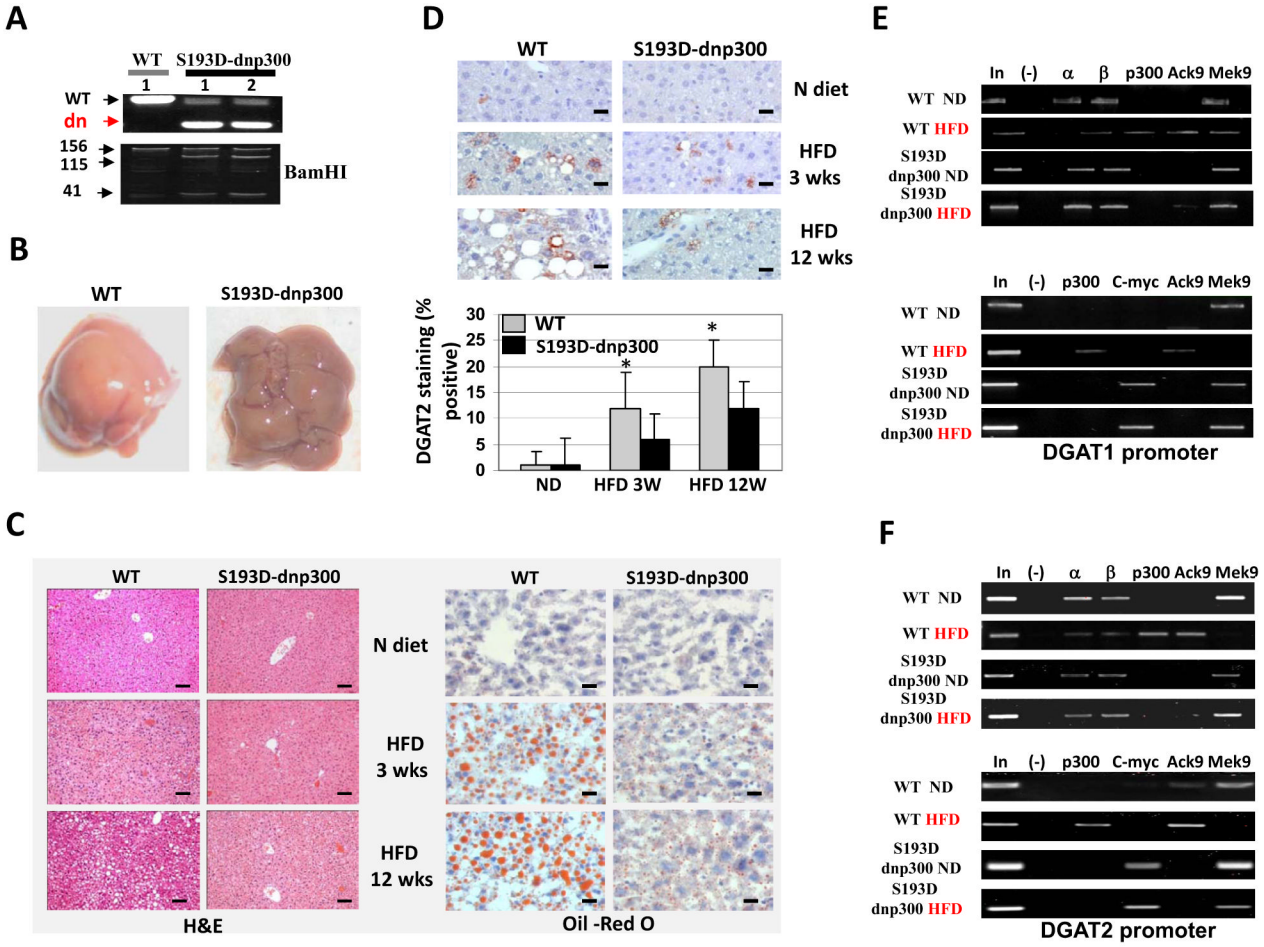

Figure 6.

Dnp300 inhibits development of steatosis in S193D mice. **A.** Genotyping of the double S193D-dnp300 mice. The picture shows PCR-based genotyping of dnp300 and digestions of the PCR products with BamHI enzyme (S193D genotyping) is shown. **B.** A typical picture of livers of WT and S193D-dnp300 mice at 12 weeks after initiation of HFD. **C.** H&E and Oil Red O staining of the livers. Scale bar of H&E staining: 40 μm. Scale bar of Oil Red O staining: 10 μm. **D.** Expression of DGAT2 in livers from WT and S193D-dnp300 mice. Bar graphs show number of DGAT2-positive hepatocytes as an average of three repeats with three mice of each genotype. **E and F.** Examination of the p300-C/EBPα/β complexes on the DGAT1 and DGAT2 promoters using the ChIP assay. The ChIP was performed as described in the legend to Fig. 2C.

NIH-PA Author Manuscript

NIH-PA Author Manuscript

NIH-PA Author Manuscript

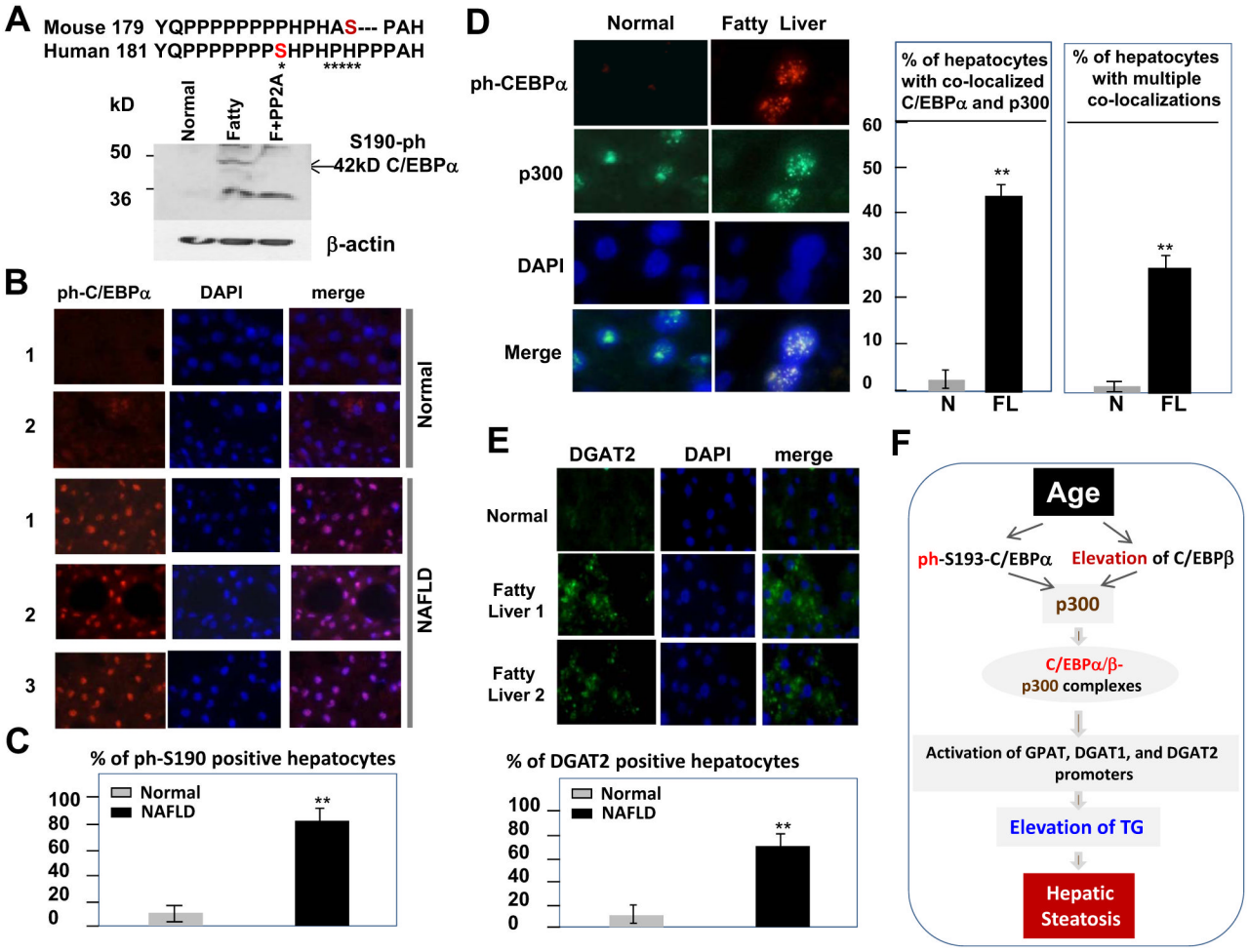

Figure 7.

C/EBPα-p300-DGAT1/2 pathway is elevated in livers of patients with non-alcoholic fatty liver disease. **A.** Generation of antibodies to human p-Ser190 isoform of C/EBPα. Sequences of mouse and human C/EBPα surrounding Ser193 and Ser190 are shown. Asterisks show differences in the sequences. Bottom: Western blotting with antibodies to p-Ser190 human C/EBPα. F+PP2A; proteins from patients with fatty liver were treated with phosphatase PP2A. **B.** Immunostaining of normal livers and livers from patients with fatty liver diseases using antibodies to p-Ser190 isoform of C/EBPα. The slides were stained with DAPI. **C.** Percentage of p-Ser190-C/EBPα positive hepatocytes in livers of normal patients and in livers of patients with fatty liver disease. **D.** Amounts of p-Ser190–C/EBPα-p300 complexes are increased in livers of NAFLD patients. The same liver sections were stained with antibodies to p-Ser190-C/EBPα, to p300, and with DAPI. Merge shows colocalization of C/EBPα and p300 in nucleus. Bar graphs show total number of hepatocytes with colocalization of C/EBPα and p300 and number of hepatocytes with multiple foci of colocalizations. **E.** Amounts of DGAT2 are increased in livers of patients with fatty liver diseases. Liver sections were stained with antibodies to DGAT2 and with DAPI. Bar graphs show percentage of DGAT2-positive hepatocytes. **F.** A model showing hypothetical mechanisms for the age-associated hepatic steatosis.